Regulation of the magnetic behavior by adjusting oxygen stoichiometry in ZrO_x film

Huanfeng Zhu (朱焕锋)[1], Jing Li (李 晶)[1,2,*], Kun Chen (陈 坤)[1], Xinyu Yi (易歆雨)[1], Shuai Cheng (程 帅)[1], Yafei Yuan (袁亚飞)[1], and Fuxi Gan (干福熹)[1]

[1]*Shanghai Ultra-Precision Optical Manufacturing Engineering Center, Department of Optical Science and Engineering, Fudan University, Shanghai 200433, China*

[2]*Key Laboratory of Micro and Nano Photonic Structure (Ministry of Education), Fudan University, Shanghai 200433, China*

**Corresponding author: lijing@fudan.edu.cn*

Received April 26, 2016; accepted September 9, 2016; posted online October 21, 2016

The mechanism of ferromagnetic ordering in ZrO_x film is investigated by both experimental observation and theoretical calculation. Magnetic measurements reveal that the magnetic properties can be adjusted from diamagnetism to ferromagnetism by varying the oxygen stoichiometry. We find that oxygen-rich defects can be responsible for the observed magnetic properties by taking the measurements of x-ray photoelectron spectroscopy and room temperature photoluminescence spectra. Density functional theory calculations further confirm that the ferromagnetic order is mainly driven by the exchange interaction between the oxygen antisites and the neighboring anion atoms.

OCIS codes: 310.4925, 050.1755, 120.7000.
doi: 10.3788/COL201614.113101.

Since the first observation of high Curie temperature ferromagnetism (FM) in Co-doped ZnO thin films[1], numerous researcher has performed theoretically and experimentally on transition metal (TM)-doped oxides diluted magnetic semiconductors (DMSs)[2]. Considerable reports have suggested that the cation defects are responsible for the observed FM[3]. On the contrary, it is proposed that anion defects can also induce FM in material systems such as ZnO[4] and SnO_2[5]. In recent years, FM was also observed in oxides doped with "nonmagnetic" elements[6] as well as undoped oxides[7], which opened an extensive controversy about whether FM is intrinsic or due to extrinsic origins such as metallic clusters and inadvertent contamination.

ZrO_2, an important semiconductor with excellent physical properties and a wide bandgap (5.1–7.8 eV), has attracted great attention for its potential applications in electronics and optoelectronics. Our interest in the ZrO_2 is motivated by recent speculation that ZrO_2 doped with Mn should be ferromagnetic above room temperature (RT), which could substantially broaden its application in the field of spintronics[8]. Several experimental works have been done to confirm the theoretical prediction. Nanocrystals with up to 5% of Mn doping in ZrO_2 synthesized by Clavel *et al.* were found to be purely paramagnetic even at low temperature[9]. Zippel *et al.*[10] had observed defect-induced FM at RT for both undoped and Mn-doped ZrO_2 thin films with up to 20 at. % Mn. However, Srivastava *et al.*[11] indicated that Y-stabilized zirconia with up to 10% of Mn were found to be paramagnetic, while 15% and 20% Mn-doped show ferromagnetic behavior due to the Mn_2O_3 secondary phase. Obviously, the field has suffered from the intense controversy on the mechanism of FM.

In many metal oxide materials, the electronic and magnetic properties can be significantly affected by the oxygen stoichiometry[12]. Study of the role of oxygen stoichiometry in these materials will be helpful in elucidating the nature and origin of fundamental interactions. In this Letter, we present our experimental and computational studies on undoped monoclinic ZrO_x thin films, aiming to shed some light on the origin of FM in this system and search for new oxide DMSs.

The ZrO_x films (~85 nm thick) used for the experiments presented in this work were deposited on silicon (111) substrates by the magnetron reactive sputtering from a pure zirconium target at RT. During deposition, the flow rate of sputtering Ar gas was fixed at 35 sccm [sccm denotes cubic centimeters per minute at standard temperature and pressure (STP)]. The oxygen stoichiometry (x) was controlled by varying the flow rates of oxygen gas during the growth. Three flow rates of reactive O_2 gas (4, 6, and 8 sccm) were used to obtain different oxygen stoichiometry in ZrO_x films. Nonmagnetic tweezers and holders were used throughout the preparation and measurement process to avoid any magnetic contamination.

The magnetic properties of sample films were measured by using a superconducting quantum interference device (SQUID) magnetometer. The chemical state of different elements present were analyzed by x-ray photoelectron spectroscopy (XPS) with Al K_α radiation (1486.6 eV) after sputtering films with Ar ions for 4 min. Shirley background subtraction was applied to all XPS data. All peaks were fitted with a Gaussian–Lorentzian function to deconvolute overlapping peaks. The photoluminescence (PL) spectra were obtained by using a photospectrometer

(Hitachi F-4500) with an excitation wavelength of 200 nm at RT.

The first-principle calculations were performed in the framework of spin-polarized density functional theory (DFT) using the projector augmented wave (PAW) as implemented in the Cambridge sequential total energy package (CASTEP)[13]. The exchange and correlation potentials were treated in the framework of a generalized gradient approximation (GGA)[14] of Perdew–Burke–Ernzerhof (PBE). The cutoff energy for the plane waves is 380 eV. A 96-atom $2 \times 2 \times 2$ monoclinic ZrO_2 supercell was used with a $2 \times 2 \times 2$ Monkhorst–Pack k-point mesh during the simulation. The geometries of the calculated supercells were optimized until the force on each atom was lower than 0.05 eV/Å.

Figure 1 shows the magnetization (M) versus field (H) curves taken on all samples carried out by using an SQUID magnetometer with an external magnetic field applied parallel to the sample's surface. The diamagnetic contribution from the silicon substrate has been subtracted from the raw data. As showed in Fig. 1(a), the magnetic properties of ZrO_x films are significantly influenced by the flow rate of oxygen gas. The magnetic measurements for the 4 sccm sample clearly exhibit weak FM at lower magnetic field values and dominate diamagnetic-like behavior at higher field values. On increasing the flow rate of oxygen gas to 6 sccm, a small signature of FM may be seen competing with the diamagnetic behavior. As for the 8 sccm sample, a weak ferromagnetic response with coercive field H_C of 80 Oe can be observed. Figure 1(b) shows the M-H curve of the 8 sccm sample measured at temperatures of 5 and 300 K. The clear hysteresis loops observed at 300 and 5 K show the typical features of FM. Moreover, they are much more significant at the low temperature of 5 K. Hence, the magnetic properties of ZrO_x film undergo a magnetic phase transition from diamagnetism to FM with an increase in the flow rates of oxygen gas from 4 to 8 sccm.

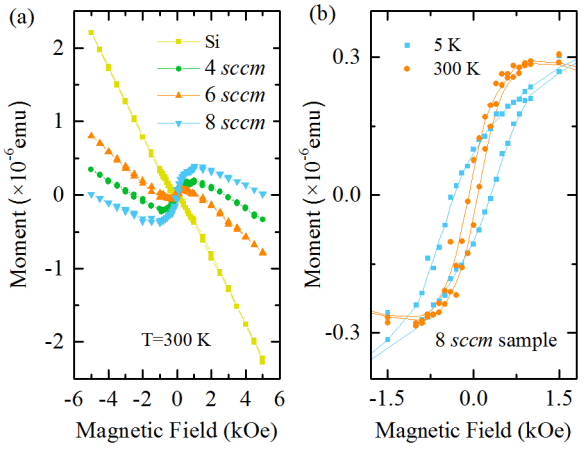

Fig. 1. (a) Magnetization versus magnetic field curves at RT for all samples. (b) Magnetic hysteresis loop for 8 sccm sample at temperatures of 5 and 300 K.

In the previous studies, native defects, especially anion vacancies, might be the main source for the observed FM in undoped oxide DMSs. To identify the existence of native defects and check if the FM in these systems is due to anion vacancies, we measured the XPS spectra. As seen from Fig. 2, the indexed peaks are corresponding to those of C, Zr, and O; no peaks due to impurity or contamination could be seen in all samples within the detection limit. Specifically, the absence of the feature peaks at 778.1, 706.6, and 640.8 eV reveals that there are no impurities of Co, Fe, and Mn elements. These observations suggest that the contribution from extrinsic pollution or impurity phase can be ignored in the case of our undoped ZrO_x films.

Figure 3(a) shows the Zr $3d$ core level XPS of the ZrO_x films. Obviously, for all the samples, the doublets Zr $3d_{3/2}$ and Zr $3d_{5/2}$ levels were measured at ~185.6 and ~183.4 eV with a spin-orbit splitting of 2.2 eV, which coincides with the results for Zr^{4+} in ZrO_2[15]. In addition, two pairs of spin-orbit-split peaks corresponding to zirconium suboxide components (Zr^{2+} and Zr^{3+}) were observed[16]. The existence of suboxide components

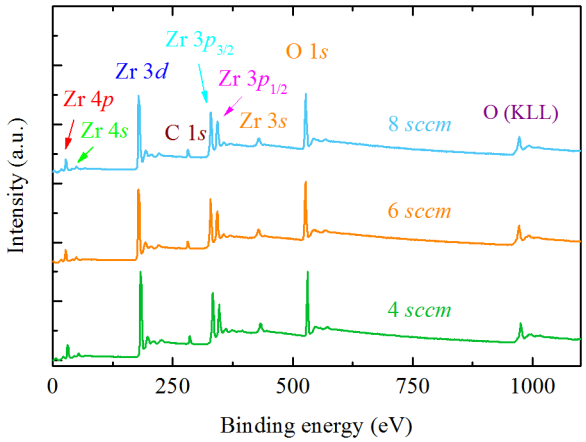

Fig. 2. Wide scan XPS spectra for ZrO_x films.

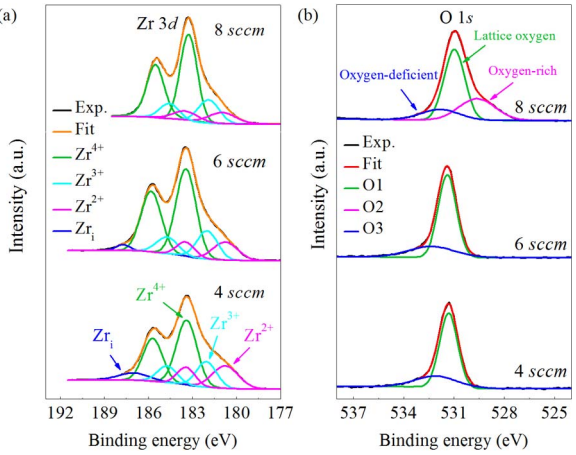

Fig. 3. (a) Zr $3d$ XPS spectra and (b) O $1s$ XPS spectra for ZrO_x films.

suggests the occurrence of reduction during the growth as the reactive formulas

$$2Zr^{4+} + O^{2-} \rightarrow V_o + 1/2O_2 + 2Zr^{3+}, \quad (1)$$

$$Zr^{4+} + O^{2-} \rightarrow V_o + 1/2O_2 + Zr^{2+}. \quad (2)$$

These observations demonstrate that some oxygen vacancies were created in order to maintain charge neutrality (as reconfirmed below). Further, the higher peak located at ~186.8 eV was observed in the 4 sccm sample and become weaker in the 6 sccm sample, but completely disappeared in the 8 sccm sample. In the present experiment, this peak is likely to be corresponding to Zr-rich defects (i.e., Zr interstitials) due to theoretical studies indicating that under oxygen-deficient growth conditions the formation enthalpy of Zr interstitial is lower than other defects but much higher in oxygen-rich conditions[17]. Since there is no ferromagnetic signal in the 4 sccm sample, in spite of the presence of Zr interstitials, it is unlikely that the FM emerges from Zr interstitials in this material.

Figure 3(b) shows the O 1*s* core level XPS of all three ZrO_x samples. The dominant peak located at ~530.9 eV (peak O1) is attributed to the lattice oxygen anions (O^{2-}) in bulk ZrO_2, whereas the shoulder peak located at ~532.2 eV (peak O3) is associated with the oxygen vacancies in the oxygen-deficient regions. Similar results were observed in TiO_2[18] and ZnO[19]. Regarding the FM signal being only observed in the 8 sccm sample while oxygen vacancies can be detected in all the samples, the oxygen-vacancy-induced FM should be excluded in the present studies. This is different from other research on undoped oxygen DMS thin films, where the ferromagnetic properties were attributed to the presence of the oxygen vacancies[5]. Conspicuously, for the 8 sccm sample, an additional peak located at ~529.6 eV (peak O2) was observed, whereas for the sample of 4 sccm and 6 sccm no XPS signals could be detected. Apparently, this new feature is directly related to the introduction of the oxygen-rich defects, such as oxygen antisites (O_{Zr}) and/or oxygen interstitials (O_i). Thus, it is reasonable to anticipate that the O_{Zr} and/or O_i instead of V_O play a pivotal role in mediating the FM in ZrO_x films.

To substantiate the above proposed assumption, PL measurements were employed. Figure 4 shows the PL spectra of the ZrO_x films obtained using an excitation wavelength of 200 nm (6.19 eV). For the 8 sccm sample, several emission peaks are observed at around 290, 318, 361, and 557 nm, which are tentatively denoted as A, B, C, and D, respectively. It is noticeable that the intensity of the emission peak depends markedly on the growth ambient, abruptly increasing as the oxygen concentration increases. In an ideal ZrO_2, only Zr-O bonds exist, which will not show any luminescence. Hence, the observed luminescence from our samples should be related to the energy level induced by the presence of defects in the ZrO_x samples. The emission peak A originated from the radiative decay of intrinsic self-trapped excitations,

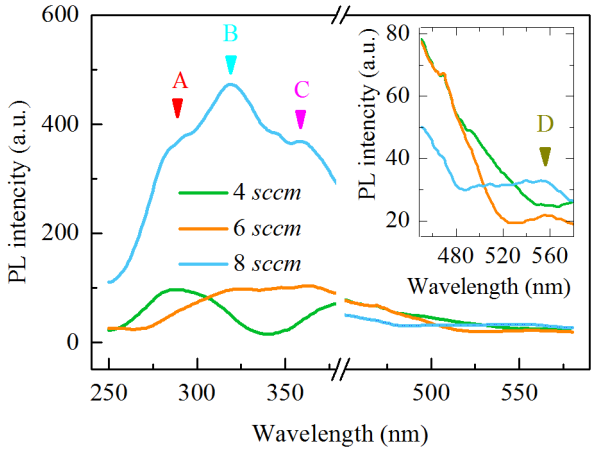

Fig. 4. PL spectra of ZrO_x films measured at RT. The inset shows an enlarged visible wavelength region of 450–580 nm.

while C can be ascribed to electrons neutralized with the holes trapped in the luminescence centers of Zr^{2+} and Zr^{3+}[20]. The origin of the emission peak D is generally assigned to the surface defects and oxygen vacancies[21]. The emission peak B, where the luminescence intensity is suppressed in oxygen-deficient samples, is likely attributed to oxygen-rich defects (i.e., O_i and O_{Zr}) in ZrO_2. Thus, according to the XPS and PL results, we believe that a sufficient amount of oxygen-rich defect is essential to produce the FM in the ZrO_x films.

Next, the first-principle spin-polarized DFT was performed in order to further identify the defect-induced magnetism in *m*-ZrO_2 system. The pure *m*-ZrO_2 was chosen to start the investigation (see Fig. 5). The total density of states (DOS) and partial density of states (PDOS) for *m*-zirconia is shown in Figs. 6(a) and 6(b), respectively. It is found that the valence band is primarily composed of O *p* states, whereas the conduction band mainly comes from Zr *d* states. The calculated bandgap for *m*-ZrO_2 is 3.6 eV, which is in good agreement with other calculations[22]. However, the calculated bandgap is much lower than the experimental value[23], which can be attributed to the poor description of the strong

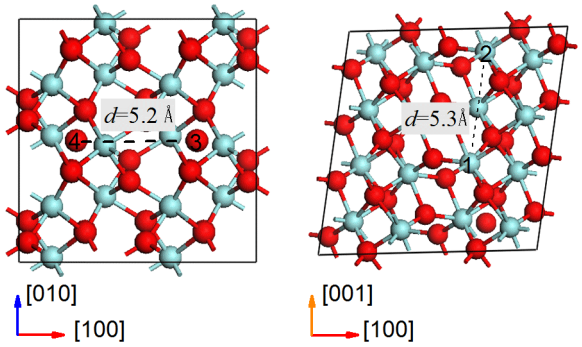

Fig. 5. 2 × 2 × 2 supercell of monoclinic ZrO_2. The red and cyan spheres represent the O and Zr atoms, respectively. The positions of Zr atoms substituted by O atoms are denoted by 1 and 2, while the O interstitials are marked by 3 and 4.

Coulomb correlation and exchange interaction between electrons in the GGA approximation.

As mentioned above, oxygen-rich defects play an important role in the magnetic properties of the ZrO_2 system. For this reason, we focus on the magnetic behaviors of the O_i and O_{Zr} in ZrO_2. In Figs. 6(c)–6(f), the DOS and PDOS of ZrO_2 with different O_i concentrations were calculated. It is observed from these figures that the conduction band of m-ZrO_2 with the O_i defect is shifted to lower energy and some partially occupied states are introduced in the bandgap. Note that the states in the valence band are occupied, while those of the conduction band are empty. These results imply that there is an increase in the number of holes and a decrease in the number of electrons. It can be seen that there is symmetry between up and down spin in both the conduction and valence bands, so there was no appearance of magnetism.

Now, we concentrate on the magnetism of O by substituting Zr in the m-ZrO_2 system. When one Zr atom is replaced by an O atom (3 at. %), the calculated results show that some localized band-ap states introduced by the O_{Zr} defect are found in the bandgap [see Fig. 7(a)]. Further PDOS [Figs. 7(b)] indicates that these localized impurity states consist of the spin-polarized states of O_{Zr} and its neighboring O ions. Interestingly, the PDOS of the O_{Zr} and its neighboring O ions both are spin polarized. However, their magnetic moments are in opposite directions, which results in a zero total magnetic moment.

However, as the concentration of O_{Zr} increases from 3% to 6% the magnetic moment increases significantly from

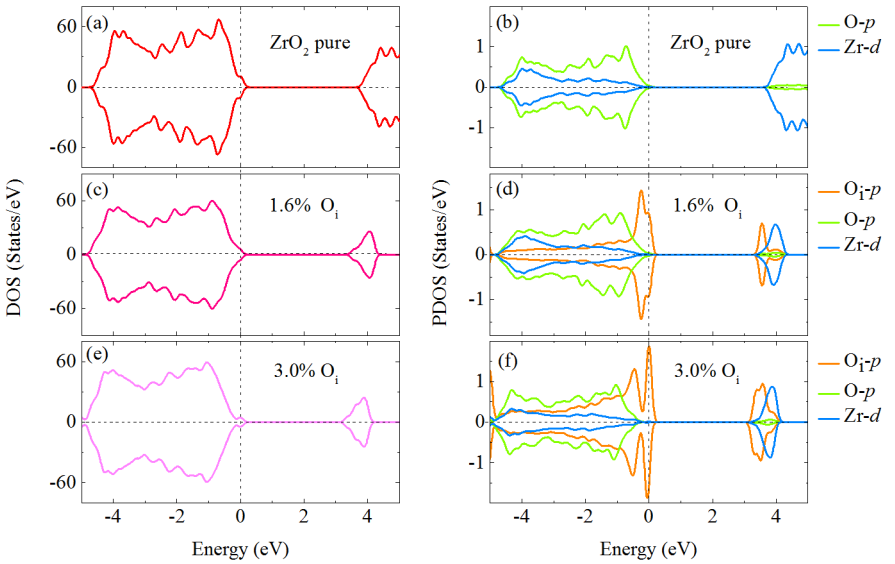

Fig. 6. DOS and PDOS of the (a)–(b) pure m-ZrO_2, (c)–(d) 1.6%, and (e)–(f) 3% oxygen interstitial defects in m-ZrO_2. The vertical dotted line stands for the Fermi level.

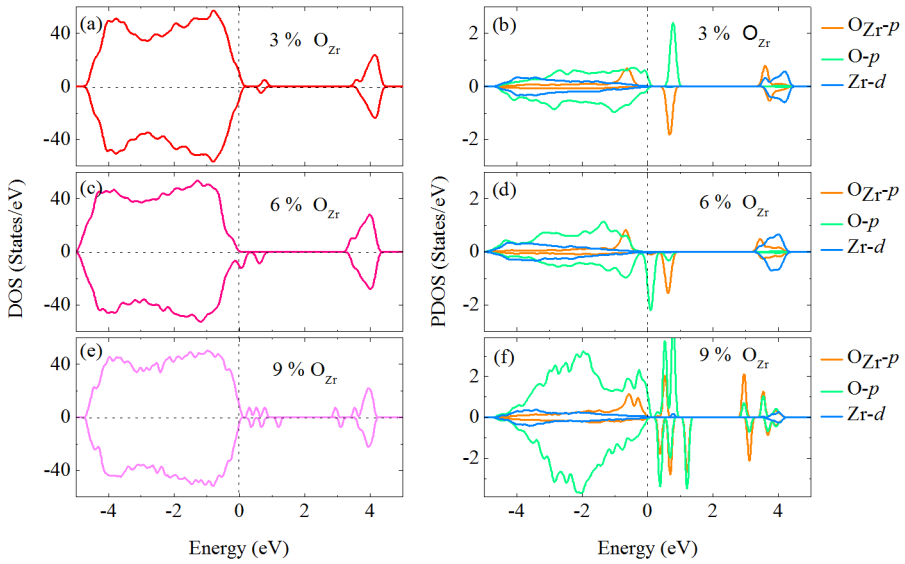

Fig. 7. DOS and PDOS of m-ZrO_2 with O_{Zr} concentration of (a)–(b) 3%, (c)–(d) 6%, and (e)–(f) 9%. The vertical dotted line stands for the Fermi level.

almost zero to 1.98 μ_B. To further make out the origin of the magnetic moments, the DOS and PDOS of O_{Zr} 2p and its neighboring O 2p and Zr 4d in the 6% of O_{Zr} are presented in Figs. 7(c)–7(d). One can see clearly that the spin-up states are fully occupied but the spin-down states are partially filled, which indicates that the system is half metallic and shows an intrinsic p-typed ferromagnetic behavior. The unoccupied states around the Fermi level are mainly dominated by the O 2p states nearing the O_{Zr} atoms. Moreover, it is found that O_{Zr} induced the impurity bands about 0.7 eV above the valance band maximum, which makes O_{Zr} a deep acceptor. These states originated from the localized 2p orbitals of the O_{Zr} ions and they have stronger p-p hybridization with the neighboring O 2p states. Such a strong p-p interaction results in a 0.3 eV splitting between the majority- and minority-spin states near the Fermi level, implying the ferromagnetic coupling can be mediated by the high concentration of holes introduced by O_{Zr}. By this p-p interaction, holes mediate the spin alignment of O atoms, leading to an indirect ferromagnetic coupling of O atoms.

With further increase of the concentration of O_{Zr} to 9% in the supercell, the magnetic moment decreases to 0.0023 μ_B. The reason can be explained as follows. For 6% of O_{Zr}, there exists ferromagnetic coupling between the O_{Zr} 2p states and its neighboring O 2p states. On increasing the concentration, the nature of the coupling changes, and there exists an anti-ferromagnetic coupling between O_{Zr} 2p states and its neighboring O 2p states, as shown in Figs. 7(e) and 7(f). Due to the change in the nature of the coupling, the value of the total magnetic moment decreases upon increasing the concentration from 6%. In addition, the cases of the V_O were also calculated, and we found that no matter how many and where the V_O vacancies were, they exhibited a zero net magnetic moment of the systems, consistent with the experimental results. Therefore, we conclude that the hole-mediated p-p coupling interaction between the O_{Zr} defects and the neighboring O atoms plays the major role in forming the FM in the ZrO_x films.

In conclusion, the experimental results reveal that the magnetic properties of ZrO_x films can be regulated by varying the flow rate of oxygen gas during the growth process, and oxygen-rich defects instead of oxygen vacancies play a vital role in developing the ferromagnetic order. First-principle calculations further indicate that the FM should arise from the O_{Zr} and the neighboring O atoms, due to the p-p coupling interaction between them. Moreover, this ferromagnetic coupling can be mediated by the hole concentration. This work provides a significant understanding of the origin of FM in undoped oxide DMSs, and may open up a new opportunity for future spintronic device applications.

This work was supported by the National Nature Science Foundation of China (No. 60578047), the National Basic Research Program of China (Nos. 2009CB929201 and 2012CB934303), the National Science and Technology Major Project of the Ministry of Science and Technology of China (No. 2011ZX02402), the Nature Science Foundation of Shanghai (No. 13ZR1402600), and the Shanghai Commission of Science and Technology (Nos. 06DJ14007 and 11DZ2282200).

References

1. Y. Matsumoto, M. Murakami, T. Shono, T. Hasegawa, T. Fukumura, M. Kawasaki, P. Ahmet, T. Chikyow, S.-Y. Koshihara, and H. Koinuma, Science **291**, 854 (2001).
2. T. Ohtsuki, A. Chainani, R. Eguchi, M. Matsunami, Y. Takata, M. Taguchi, Y. Nishino, K. Tamasaku, M. Yabashi, T. Ishikawa, M. Oura, Y. Senba, H. Ohashi, and S. Shin, Phys. Rev. Lett. **106**, 047602 (2011).
3. M. Khalid, M. Ziese, A. Setzer, P. Esquinazi, M. Lorenz, H. Hochmuth, M. Grundmann, D. Spemann, T. Butz, G. Brauer, W. Anwand, G. Fischer, W. A. Adeagbo, W. Hergert, and A. Ernst, Phys. Rev. B **80**, 035331 (2009).
4. X. Y. Xu, C. X. Xu, J. Dai, J. G. Hu, F. J. Li, and S. Zhang, J. Phys. Chem. C **116**, 8813 (2012).
5. N. H. Hong, N. Poirot, and J. Sakai, Phys. Rev. B **77**, 033205 (2008).
6. H. Zhu, J. Li, K. Chen, X. Yi, S. Cheng, and F. Gan, Sci. Rep. **5**, 8586 (2015).
7. N. Selvi, S. Sankar, and K. Dinakaran, J. Mater. Sci. Mater. Electron. **26**, 273 (2015).
8. S. Ostanin, A. Ernst, L. M. Sandratskii, P. Bruno, M. Dane, I. D. Hughes, J. B. Staunton, W. Hergert, I. Mertig, and J. Kudrnovsky, Phys. Rev. Lett. **98**, 016101 (2007).
9. G. Clavel, M. G. Willinger, D. Zitoun, and N. Pinna, Eur. J. Inorg. Chem. **2008**, 863 (2008).
10. J. Zippel, M. Lorenz, A. Setzer, G. Wagner, N. Sobolev, P. Esquinazi, and M. Grundmann, Phys. Rev. B **82**, 125209 (2010).
11. S. K. Srivastava, P. Lejay, B. Barbara, O. Boisron, S. Pailhes, and G. Bouzerar, J. Appl. Phys. **110**, 043929 (2011).
12. Y. B. Nian, J. Strozier, N. J. Wu, X. Chen, and A. Ignatiev, Phys. Rev. Lett. **98**, 146403 (2007).
13. M. D. Segall, P. J. D. Lindan, M. J. Probert, C. J. Pickard, P. J. Hasnip, S. J. Clark, and M. C. Payne, J. Phys. Condens. Matter **14**, 2717 (2002).
14. J. P. Perdew, K. Burke, and M. Ernzerhof, Phys. Rev. Lett. **77**, 3865 (1996).
15. S. A. Steiner, T. F. Baumann, B. C. Bayer, R. Blume, M. A. Worsley, W. J. MoberlyChan, E. L. Shaw, R. Schlogl, A. J. Hart, S. Hofmann, and B. L. Wardle, J. Am. Chem. Soc. **131**, 12144 (2009).
16. W. C. Liao, T. Zheng, P. Wang, S. S. Tu, and W. Q. Pan, J. Environ. Sci (Beijing, China) **22**, 1800 (2010).
17. S. J. Zhao, J. M. Xue, Y. G. Wang, and S. Yan, J. Appl. Phys. **111**, 043514 (2012).
18. Y. Yu, K. J. Wu, and D. L. Wang, Appl. Phys. Lett. **99**, 192104 (2011).
19. K. Chen, H. Zhu, X. Yi, S. Cheng, J. Li, S. Wang, M. Lu, M. Xu, L. Ma, and L. Lv, Chin. Opt. Lett. **13**, 103101 (2015).
20. J. S. Lakshmi, I. J. Berlin, G. P. Daniel, P. V. Thomas, and K. Joy, Phys. B **406**, 3050 (2011).
21. A. K. Singh and U. T. Nakate, Sci. World J. **2014**, 349457 (2014).
22. T. Archer, C. D. Pemmaraju, and S. Sanvito, J. Magn. Magn. Mater. **316**, E188 (2007).
23. P. Aldebert and J. P. Traverse, J. Am. Ceram. Soc. **68**, 34 (1985).